

Chapter 8

Experimental Studies of Plasmonic Nanoparticle Effects on Organic Solar Cells

Dixon D. S. Fung and Wallace C. H. Choy

Abstract The incorporation of plasmonic nanoparticles (NPs) into different layers of organic solar cells (OSCs) is studied in this chapter. First, we incorporate NPs into the hole collection layer of OSCs. The resulting improvements in Power Conversion Efficiency (PCE) are found to originate mainly from improvement in hole collection efficiency, while Localized Surface Plasmon Resonance (LSPR) effects are found to have negligible effect on active layer absorption. Next, we incorporate NPs into the active layer of OSCs. In this case, the absorption of the active layer improves, but we also showed that consideration of electrical properties including carrier mobility, exciton dissociation efficiency, and active layer morphology is required to account for the PCE trend. In both studies, we theoretically show that the very strong near field of NPs is found to distribute laterally along the layer in which the NPs are incorporated in, and hence leading to active layer absorption improvements only when NPs are incorporated into the active layer. Lastly, we incorporated NPs into both active layer and hole collection layer in which the accumulated effects of NPs in the different layers achieved $\sim 22\%$ improvement in PCE as compared to the optimized control OSCs using poly (3-hexylthiophene): phenyl-C61-butyric acid methyl ester (P3HT:PCBM) as the active layer.

D. D. S. Fung · W. C. H. Choy (✉)
Department of Electrical and Electronic Engineering, The University of Hong Kong,
Pokfulam, Hong Kong
e-mail: chchoy@eee.hku.hk

8.1 Introduction

Plasmonics has been proposed for various interesting applications including bio-sensing [1], waveguides [2], optical cloaking [3], and quantum computing [4]. Recently, the ability of plasmonic structures to greatly enhance electric fields has attracted attention in the field of organic solar cells (OSCs), in which material absorption is a crucial factor that has to be improved.

Incorporation of plasmonic structures on solar cells could potentially improve its efficiency through three possible optical effects [5]. First, metallic nanoparticles (NPs) can scatter the incident light into waveguide modes in the active layer of the solar cell, increasing the optical path distance and improving absorption. Second, by utilizing the Localized Surface Plasmon Resonance (LSPR) effect, the NPs can be mixed into the OSC during fabrication and act as antennas, creating a very strong near field around the NPs and enhancing absorption of the active layer. Third, using a nanostructured metallic electrode such as a grating, surface plasmon resonance (SPR) can be excited and increase the field near the dielectric/metal interface, thus improving absorption in the solar cell.

There has been great interest in the applications of plasmonic structures on OSCs to improve power conversion efficiency (PCE) in recent years. By conveniently mixing NPs into the hole collection layer of OSCs, reports have claimed that LSPR effects improved the absorption hence the efficiency of OSCs. [6–9] On the other hand, Heeger et al. have incorporated Au NPs into the active layer of solar cells and showed the wide-band improvement of absorption in poly(3-hexylthiophene): phenyl-C61-butyric acid methyl ester (P3HT:PCBM) is due to scattering of NPs instead of LSPR effects [10]. Ag NPs and nanowires were also demonstrated to improve absorption and PCE by addition into the active layer [11, 12]. Evaporation of a very thin layer of Au or Ag forms small clusters of metals which also exhibit LSPR effects and are used in solar cells [8]. On the other hand, various other nanostructures have also been used to improve absorption and PCE [13, 14].

On the electrical properties of NP-doped solar cells, an early report of NPs incorporated into solar cells has stated that the increase of solar cell performance may be due to the introduction of dopant states which increases the electrical conductivity of the active layer [15]. Incorporation of Ag nanowires into the active layer of OSCs has been shown to increase both hole and electron mobility, but the detailed physics was not investigated in depth [11]. There have also been reports on changes in open circuit voltage (V_{OC}) when NPs are incorporated into OSCs [10]. On the other hand, Wu et al. have reported an increase in exciton dissociation probability of OSCs incorporated with NPs and claimed that this increase is due to interactions between plasmons and photogenerated excitons [7].

In the mentioned reports, PCE improvements in OSCs incorporating NPs have been well demonstrated but the investigations in device mechanisms have been lacking in depth. In particular, the actual role of LSPR effects has not been well clarified and questions could still be raised about whether LSPR is actually improving device performances. On the other hand, as plasmonic nanostructures

are commonly incorporated in-side an OSC, their effects on the electrical properties of OSCs are likely equally important as optical properties. Previous reports have studied optical effects of the NPs, while the impact of NPs on the electrical properties of OSCs is still unclear. The understanding on the electrical properties of OSCs is important for optimizing the plasmonic OSCs and open new applications of plasmonic nanostructures.

In this chapter, detailed studies in the device mechanisms of OSCs will be described when NPs are incorporated into various positions through experiment and theoretical simulations. The objectives are (1) clarify the extent that LSPR improves absorption in active layer; (2) describe the difference in the role of LSPR effects when NPs are incorporated into the hole collection layer or active layer; (3) study the device mechanisms, apart from optical effects, that will be changed when NPs are incorporated; and (4) describe the large efficiency improvements in OSCs by incorporation of NPs in all organic layers.

8.2 Electrical and Optical Properties of Organic Solar Cells with Au Nanoparticles Doped into the PEDOT:PSS Layer

Considering the origin of performance improvement after addition of NPs, the effects of doping the poly(3,4-ethylenedioxythiophene) poly(styrenesulfonate) (PEDOT:PSS) layer of a OSC with Au NPs have been reported [36]. In the report, monofunctional poly(ethylene glycol) (PEG)-capped Au NPs with average diameter of 18 nm are doped into the PEDOT:PSS hole collection layer of an optimized OSC with P3HT:PCBM as the active layer, leading to $\sim 13\%$ peak PCE improvement. The effect of PEG capping on Au NPs has also been investigated from a device fabrication perspective. Together with theoretical simulations which are discussed in Chap. 7 [16], the effects of Au NPs on the optical and electrical properties of OSCs have been studied. The results show that the competition between improved hole collection at the PEDOT:PSS/active layer interface and reduced exciton quenching, at donor/acceptor junctions, instead of the LSPR effect, are major contributors to the measured PCE variation.

8.2.1 Performances of the Au NP Devices

The current density (J) versus voltage (V) characteristics of devices with structure ITO/PEDOT:PSS(with PEG-capped Au NPs)/P3HT:PCBM/LiF(1 nm)/Al(100 nm) incorporating various Au NP concentrations in PEDOT:PSS layer is shown in Fig. 8.1 and the device characteristics are summarized in Table 8.1.

It is shown that increasing Au NPs concentration in PEDOT:PSS improves PCE of our OSCs, peaking at 0.32 wt% with PCE of 3.51 % which corresponds to

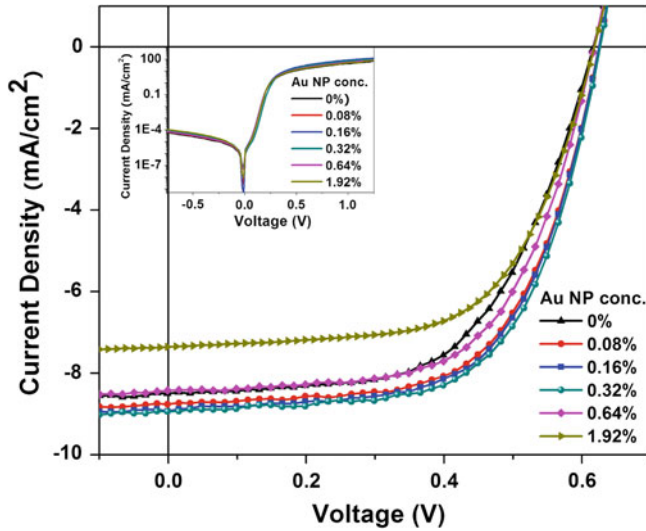


Fig. 8.1 J - V characteristics of solar cells with structures ITO/PEDOT:PSS (with PEG-capped Au NPs)/P3HT:PCBM/LiF (1 nm)/Al(100 nm), incorporated with different NP concentrations under AM 1.5G illumination at 100 mW/cm^2 . Inset Dark J - V characteristics of the solar cells [18]

Table 8.1 Device performances for solar cells with structure ITO/PEDOT:PSS(with PEG-capped Au NPs)/P3HT:PCBM/LiF(1 nm)/Al(100 nm), incorporated with different NP concentrations [18]

NP conc. (wt %)	J_{sc} (mA/cm 2)	V_{OC} (V)	FF (%)	PCE (%)
0	8.5 ± 0.19	0.62 ± 0.01	58 ± 1.3	3.10 ± 0.10
0.08	8.77 ± 0.23	0.63 ± 0.01	61 ± 1.0	3.40 ± 0.11
0.16	8.93 ± 0.19	0.63 ± 0.01	61 ± 1.1	3.46 ± 0.10
0.32	8.94 ± 0.15	0.63 ± 0.01	62 ± 1.0	3.51 ± 0.09
0.64	8.56 ± 0.11	0.62 ± 0.01	61 ± 1.2	3.21 ± 0.10
1.92	7.36 ± 0.2	0.62 ± 0.01	61 ± 0.5	2.80 ± 0.13

$\sim 13\%$ improvement. Improvements originate from increases in FF and J_{sc} , from 0.58 to 0.62 and 8.5–8.94 mA/cm 2 , respectively. Further, increasing the concentration of NPs has detrimental effect on device performances, with PCE dropping to 2.80% at 1.92 wt% Au NPs concentration. From the dark J - V characteristics in the inset of Fig. 8.1, no significant change in leakage current is observed after incorporation of Au NPs. The underlying physics of the PCE trend can be explored by studying the optical and electrical properties as described the following sections.

8.2.2 Au NP Properties and the Effects of PEG

The absorption spectrum of Au NPs without PEG in water is shown in Fig. 8.2. The absorption peak at ~ 520 nm corresponds to the excitation of LSPR. Coating PEG onto Au NPs has no discernable effect on the peak position of optical absorption. The average diameter of Au NPs is approximately 18 nm, based on TEM measurements, as shown in the inset of Fig. 8.2.

Regarding the effects of Au NPs with or without PEG coating on device performances, for the same concentration (0.32 wt%) of Au NPs, PCE of the device with Au NP (PEG) improves from 3.1 (control device without Au NPs) to 3.51 %, while devices with Au NP (no PEG) show no performance improvement for the same device structure of ITO/PEDOT:PSS:Au NPs/P3HT:PCBM/LiF(1 nm)/Al(100 nm) was fabricated to investigate the device performance. The origin of this effect can be further elaborated from SEM images taken on PEDOT:PSS:Au NP films. As shown in Fig. 8.3a, Au NPs with PEG are well dispersed in a PEDOT:PSS:Au NP film with no clear aggregation, while Au NPs without PEG aggregate into clumps of NPs in a film (Fig. 8.3b). This can be explained by the positive surface charge [17] of the Au NPs generated in the synthesis process [18], while PSS molecules are anionic in nature [19]. When Au NPs are added to PEDOT:PSS solution, the adsorption of anionic PSS molecules on positively charged Au NPs leads to the aggregation of Au NPs. On the other hand, the PEG capping layer has a shielding effect on Au NPs, leading to reduce interaction of NPs with the surrounding medium. Meanwhile, PEG itself does not have any effect other than the prevention of Au NP aggregation [20], this is confirmed from the devices with and without PEG (2 mg/ml) dissolved into the PEDOT:PSS layer and

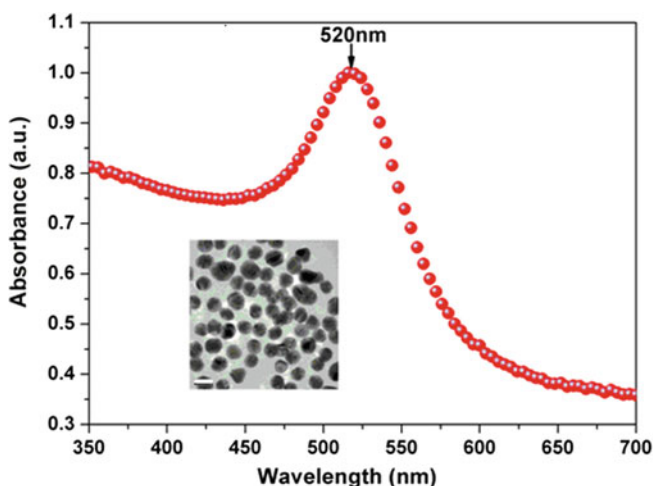


Fig. 8.2 Absorption spectrum of Au NPs in water. *Inset* is the TEM image of the NPs. The white bar is approximately 20 nm long [18]

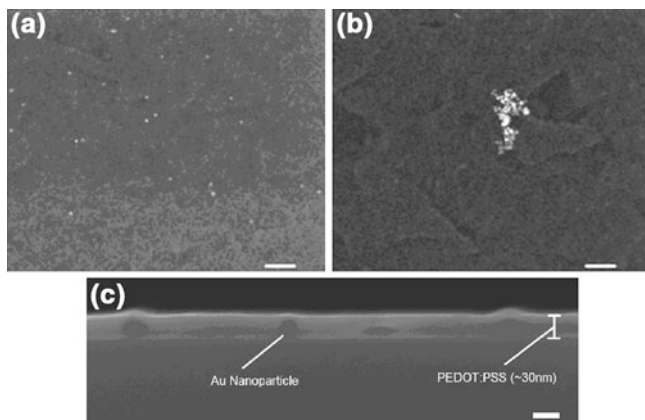


Fig. 8.3 SEM images of the surface of PEDOT:PSS:Au NPs films with **a** Au NPs capped with PEG, **b** Au NPs not capped with PEG. The *white bars* in **(a)** and **(b)** are approximately 200 nm long. **c** SEM image of the cross-section of a PEDOT:PSS:Au NPs film, with Au NPs capped with PEG. The *white bar* in **(c)** is approximately 30 nm long. Note that the image is focused on the cross-section surface of PEDOT:PSS and the Au NPs might be out of focus [18]

observed no discernible difference in the performance. Therefore, PEG itself does not exert any significant effects on our device performances. The contribution of PEG is to prevent formation of aggregation sites and allow the uniform dispersion of Au NPs. In the following discussion, the effects of PEG capped Au NPs on OSCs will be described.

The positioning of Au NPs along with the vertical profile of the PEDOT:PSS film is shown in Fig. 8.3c. It can be seen that the majority of the bulk of individual NPs are located within the PEDOT:PSS layer. At the locations of Au NPs, bumps are created on the surface of PEDOT:PSS. However, the Au NPs at the bumps are covered by a layer of PEDOT:PSS and no bare Au NP protrusions are reported in measurements.

8.2.3 Plasmonic Effects

The LSPR effects can be investigated from the absorption spectrum of the PEDOT:PSS/P3HT:PCBM films, with or without Au NPs in PEDOT:PSS as shown in Fig. 8.4a. Interestingly, no significant difference is observed in absorption between the samples with and without Au NPs. Theoretical studies [16] have also been conducted to understand plasmonic effects of Au NPs in the devices [18]. The theoretical enhancement factor (i.e., the ratio of the active layer light absorption of the PEDOT:PSS:Au NPs device over that of the conventional PEDOT:PSS one) shows no clear absorption enhancement, with a value around 1 as shown in the inset of Fig. 8.4a which agrees well with the experimental results.

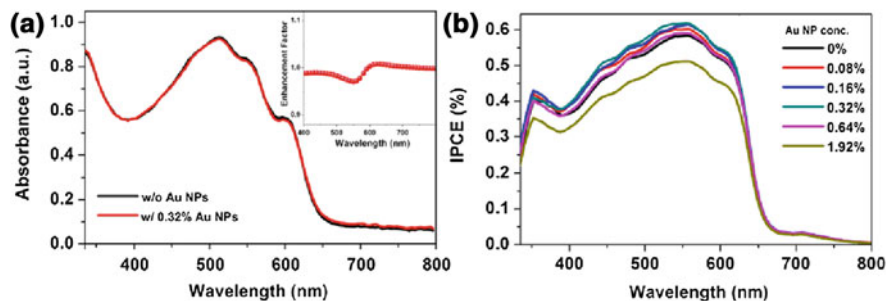


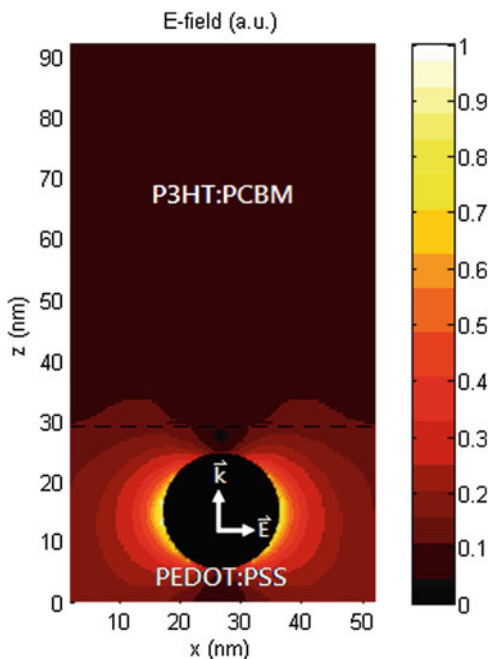
Fig. 8.4 **a** Absorbance of PEDOT:PSS/P3HT:PCBM film with or without Au NPs incorporation (0.32 wt%); *inset* of **(a)**: theoretical absorption enhancement factor (detailed model shown in [Appendix A](#)); **b** IPCE of the solar cells with various Au NP concentrations in PEDOT:PSS [18]

LSPR is at about 580 nm, although the enhancement is weak. The theoretical results and reflectance measurements also show that the Al electrode does not obviously affect the LSPR effect on the absorption enhancement as the Al electrode is situated far (220 nm) from the PEDOT:PSS layer.

The reason for the small optical enhancement is that when light is incident in normal into the device through ITO, the very strong near field around Au NPs due to LSPR mainly distributes laterally along the PEDOT:PSS layer rather than vertically into the adjacent active layer as shown in [Fig. 8.5](#). As a result, no clear light absorption enhancement can be obtained in the active layer of P3HT:PCBM. Importantly, the understanding can also be applied to other cases with the metallic NPs (such as Ag, Pt etc.) incorporated into the buffer layer adjacent to the active layer of typical organic thin-film solar cells due to the lateral distribution feature of the strong near-field. Meanwhile, the work suggests that near-field physics needs to be accounted for in the optical design of photovoltaics, and some traditional physical quantities, such as scattering cross-section, are not enough to fully characterize the optical properties of OSCs. For instance, typically, scattering cross-section is very useful to locate the plasmonic resonance region and determine the strength of scattering [21, 22]. However, it cannot provide the directional properties of electric field, and thus the direction dependence of absorption enhancement.

Although there is no obvious enhancement in the light absorption of the active layer, IPCE of our PEDOT:PSS: Au NPs devices increases with Au NP concentration and the 0.32 wt% device shows the highest IPCE, with $\sim 64\%$ at 550 nm as shown in [Fig. 8.4b](#). For higher Au NP concentrations, IPCE decreases. This is in good agreement with the trend of J_{sc} . The apparent discrepancy between light absorption and IPCE can be explained by the fact that IPCE measures the percentage of incident photons that eventually results in free charges being collected through the OSC electrodes. Factors beyond light absorption, such as the resistance of electrodes, exciton dissociation rate, and charge collection efficiencies will also affect the magnitude of IPCE. However, such nonoptical effects are likely to be not wavelength sensitive and are represented by vertical shifts of the entire

Fig. 8.5 Theoretical electric field profile in the PEDOT:PSS: Au NPs/ P3HT:PCBM OSCs [18]



IPCE spectrum. Comparing devices with or without Au NPs in Fig. 8.4b, it can be observed that the IPCE shows a wideband improvement from ~ 400 to 650 nm. It therefore can be concluded that plasmonic effects does not play a major role in improving PCE and electrical effects have to be accounted for.

It should be noted that in the measurement of light absorption shown in Fig. 8.4a, the absorption of the PEDOT:PSS layer (with or without Au NPs) has been deduced as they will absorb light. Therefore, the absorption spectrum represents light harvesting within the active layer only, which is important for understanding the plasmonic effects on device performances. The insignificant change in absorption spectra is a direct evidence that light absorption in P3HT:PCBM is unaffected by the incorporation of Au NPs.

8.2.4 Effects of Au NPs on PEDOT:PSS

The morphology changes of the PEDOT:PSS: Au NP layer can be observed from AFM images on a PEDOT:PSS: Au NP film for different NP concentrations as shown in Fig. 8.6. Upon increasing Au NP concentration, an obvious change can be observed in surface morphology of the PEDOT:PSS film, with an increase in roughness of ~ 5 and ~ 40 % for 0.32 and 0.64 wt% Au NPs, respectively. It has been reported that increasing anode surface roughness will increase the interface area between the anode and active layer, providing shorter routes for holes to

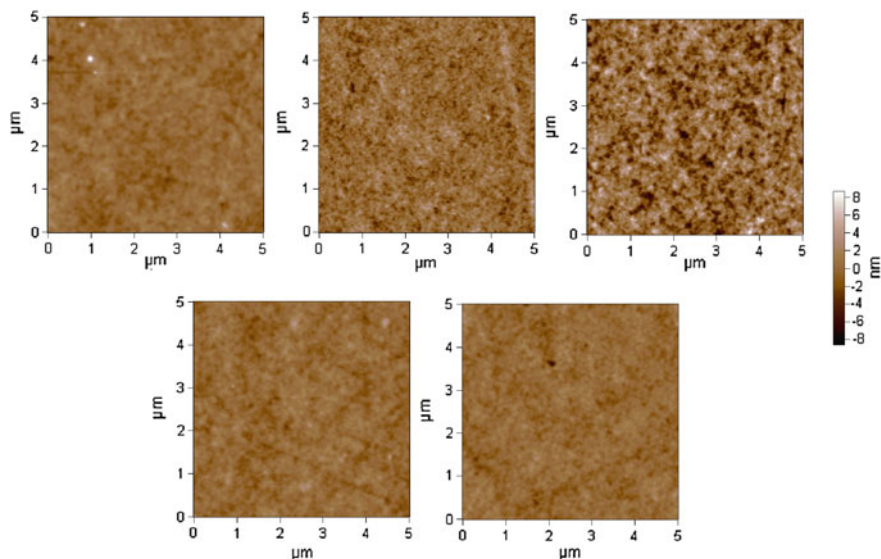


Fig. 8.6 AFM height images for different Au NP concentrations in PEDOT:PSS—0 % (*top left*), 0.32 % (*top center*), 0.64 % (*top right*). After spin-coating an extra layer of PEDOT:PSS on top of the PEDOT:PSS: Au NPs layer, the AFM images show a smoothed surface for 0.32 % (*bottom left*) and 0.64 % (*bottom right*) [18]

travel to the anode and enhancing hole collection at the anode [23]. The increased interfacial area between PEDOT:PSS and P3HT:PCBM allows the collection of a larger number of holes in the P3HT:PCBM layer, thus increasing J_{sc} of our devices. In addition, the reduced mean distance of between generated holes and the PEDOT:PSS interface diminishes the dependence of holes on the external electric field for collection at the anode, explaining the improvement in FF of our devices. Besides, it has been suggested that a rough P3HT:PCBM surface creates defect sites that assist exciton dissociation [24]. These effects together account for the improvements in J_{sc} and FF in our devices. The improved forward bias injection upon addition of Au NPs in our devices further support the claim that the increased PEDOT:PSS roughness increases PEDOT:PSS/P3HT:PCBM interfacial area. Considering the optical effects of a rough PEDOT:PSS surface, the transmission of PEDOT:PSS with or without Au NPs has been studied and observed no discernible difference. In addition, the refractive index difference between PEDOT:PSS and P3HT:PCBM is not large and the roughness is nanoscale. Hence, the rough PEDOT:PSS surface does not contribute to scatter light significantly.

To further elucidate this effect, an approach has been implemented to remove the surface roughness of the PEDOT:PSS layer while retaining Au NPs inside the PEDOT:PSS film. The approach is to spin-coat an extra PEDOT:PSS layer on top of the PEDOT:PSS: Au NP layer. From AFM images in Fig. 8.6, this extra layer smoothens the surface of the PEDOT:PSS to a morphology similar to a regular PEDOT:PSS layer. Devices are fabricated with the structure ITO/PEDOT:PSS: Au

NPs/PEDOT:PSS/P3HT:PCBM/LiF(1 nm)/Al (100 nm). After the insertion of the pristine PEDOT:PSS layer, the presence of Au NPs in these devices provides no improvements in device performance. Meanwhile, since optical effects have been proven to be unlikely to be a major contributor to performance improvement, one cannot argue that positive LSPR effects are diminished by the alteration of optical interference profile inside the OSC due to the addition of an extra layer of PEDOT:PSS. As a result, the main effect of the extra PEDOT:PSS layer is to smoothen the rough surface of the PEDOT:PSS:Au NPs layer. Consequently, the results indicate that the rough PEDOT:PSS: Au NPs layer surface positively contributes to device performances.

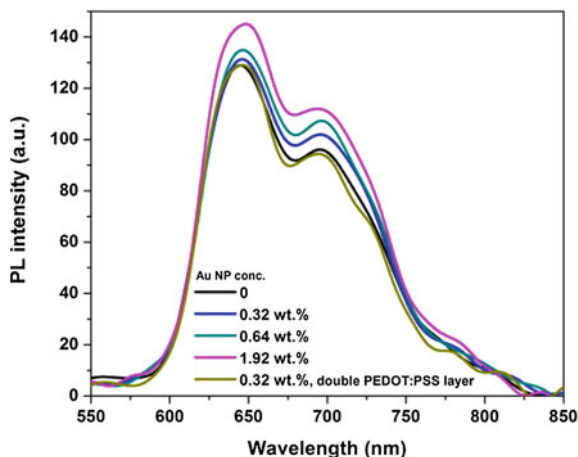
The resistance of PEDOT:PSS from resistive devices with the structure ITO/PEDOT:PSS:Au NPs/Al(80 nm) has also been reported [36]. J - V measurements from these devices indicate a slight reduction in PEDOT:PSS resistance from 1.33 (No NPs) to 0.97 Ω (0.32 wt%). Although reduction in PEDOT:PSS resistance reduces the series resistance of OSCs, the small decrease in PEDOT:PSS resistance can only provide minor contributions to device performance improvement. On the whole, it can be concluded that the improved hole collection at the roughened interface between PEDOT:PSS and P3HT:PCBM enhance device performances, while a slight reduction in PEDOT:PSS resistance by the incorporation of Au NPs can also provide minor contribution to performance improvements.

8.2.5 Effects of Au NPs on Exciton Quenching

A missing picture is the origin of device performance degradation at high NP concentrations. To investigate this effect, the photoluminescence (PL) spectrum of PEDOT:PSS:AuNPs/P3HT:PCBM films has been investigated (see Fig. 8.7). The PL spectra show increasing PL intensity upon increasing concentrations of Au NPs, with a maximum of $\sim 10\%$ increase at ~ 647 nm.

PL intensity changes can be caused by three main reasons: changes in optical absorption, exciton quenching at metal/organic interfaces [25–27], and exciton quenching at donor/acceptor (D/A) interfaces [28, 29]. The possibility of changes in optical absorption is eliminated, as we have experimentally and theoretically shown previously that light absorption of OSCs do not change significantly after the incorporation of Au NPs. Considering the second reason, exciton quenching at metal/organic interfaces, it has been reported that capping an insulating layer on Au NPs can prevent direct contact between the metal and organic layer, hence preventing exciton quenching on the NP surface [30]. Furthermore, as shown in Fig. 8.3c, Au NPs located near the surface of PEDOT:PSS are well covered by PEDOT:PSS. Hence, it is expected that the Au NPs are not in direct contact with the P3HT:PCBM layer and the effect of exciton quenching by Au NPs is negligible.

Fig. 8.7 Photoluminescence spectra of P3HT:PCBM for different Au NP concentrations in PEDOT:PSS [18]



For the third reason, the reduction in exciton quenching at D/A junctions indicates reduced D/A interface area, and hence a change in the morphology of the active layer [31]. It should be noted that studies have shown that PL increase can be a result of an increase in crystallinity of P3HT in the P3HT:PCBM blend, causing an increase in hole mobility and PCE [28, 32, 33], which apparently cannot address our results. However, it should be noted that the increase in crystallinity of P3HT has also been associated with an enhancement of absorption of P3HT:PCBM in the red region, which is not observed in the results of Ref. [18]. Hence, the increase in PL is attributed to changes in phase separation in the P3HT:PCBM blend leading to reduced D/A junction interfacial area, instead of changes in crystallinity of P3HT. The reduced D/A junction area causes exciton dissociation efficiency to decrease and reduce PCE. In addition, the AFM images of the top surface of the P3HT:PCBM film show no significant change in top surface morphology. This implies that the rough PEDOT:PSS surface, caused by the incorporation of NPs, could only cause a change in internal networking of the subsequently spin-coated P3HT:PCBM film near the PEDOT:PSS side.

Further evidence of the roughness effects on the change of phase separation can be found from the PL spectrum of PEDOT:PSS:Au NPs/PEDOT:PSS/P3HT:PCBM film (see Fig. 8.7) that no significant difference in PL intensity between the samples with single PEDOT:PSS layer (without Au NPs) and double PEDOT:PSS layer (with Au NPs in first layer) is observed. In this case, no clear PL intensity change is observed as the smoothed PEDOT:PSS surface, caused by the addition of an extra PEDOT:PSS layer, does not alter the internal networking of the active layer. Therefore, it can be concluded that incorporation of Au NPs modifies PEDOT:PSS surface morphology and leads to the reduced exciton quenching, which can be explained by alterations in the internal networking of the P3HT:PCBM film near the PEDOT:PSS side.

In terms of the impact on device performances, on the one hand, the reduction in exciton quenching after addition of Au NPs implies a reduction in free carrier

generation, leading to a lower J_{sc} and FF. On the other hand, the previously investigated hole collection improvement is advantageous to J_{sc} and FF. The competition between the two effects contributes to the trend in PCE variation as shown Table 8.1: as Au NPs are added to PEDOT:PSS, the surface roughness increases, creating a larger PEDOT:PSS/P3HT:PCBM interface area. Therefore, more holes can be collected at the anode, leading to enhancements in J_{sc} , FF and PCE. However, the increased roughness also affects P3HT:PCBM networking and reduces exciton quenching. When the Au NPs concentration increases further from 0.32 toward 1.92 %, the negative effects of reduced exciton quenching outweigh the positive effects of improved hole collection, resulting in the reduction of PCE as shown in Table 8.1 and thus PCE peaks at 0.32 wt%.

8.2.6 Section Summary

The incorporation of Au NPs into the PEDOT:PSS layer of an OSCs offers ~ 13 % improvement in PCE in robust material system of P3HT:PCBM, mainly due to improvements in J_{sc} and FF. The experimental and theoretical studies showed that absorption enhancements are minimal, and this is explained by the lateral distribution of the strong near field of NPs. The study of PEDOT:PSS morphology reveals that Au NP incorporation will cause the surface roughness of PEDOT:PSS to increase, leading to more efficient hole collection. Also, the resistance of PEDOT:PSS reduces upon incorporation of NPs. On the other hand, PL measurements indicate that exciton quenching is reduced due to the change in internal networking of the active layer. The combination of these electrical effects explains the trend of PCE reported in the work [18].

8.3 Electrical and Optical Properties of Organic Solar Cells with Au Nanoparticles Doped into the Active Layer

With our previous section showing that performance improvement of OSCs incorporated with Au NPs in the PEDOT:PSS layer is not due to LSPR effects, we would like to discuss the OSC performance improvement mechanisms when NPs are doped in a different layer and understanding the conditions in which LSPR effects can be utilized in OSCs. We noticed that previous studies have commonly used the metallic NPs as an interfacial layer on ITO coated glass substrates or a dopant of buffer layers such as PEDOT:PSS [6–9]. OSCs with the incorporation of metallic NPs into the active layer, however, have received limited detailed investigation. [12, 15, 34] Therefore, the study for further understanding both optical and electrical properties is highly desirable for OSCs with metallic NPs incorporated into the active layer.

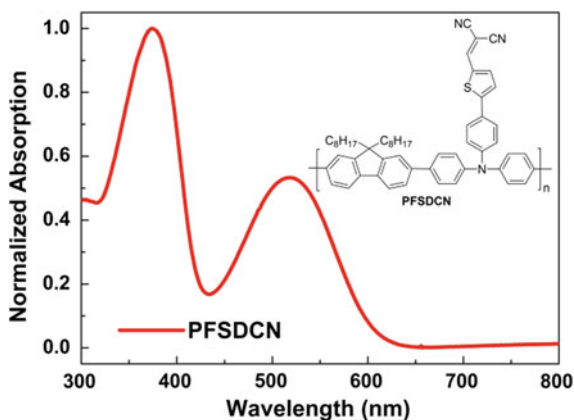
In this section, the impact of the incorporation of monofunctional PEG-capped Au NPs into the active layer of polymer blend will be discussed [35]. The polymer donor used in the active layer of the OSCs is poly[2,7-(9,9-dioctylfluorene)-*alt*-2-((4-(diphenylamino) phenyl)thiophen-2-yl)malononitrile] (PFSDCN) [36]. The improvement of V_{OC} , J_{sc} , FF is reported with an appropriate amount of Au NPs incorporated into the active layer. As a result, after optimization, the improvement of PCE by $\sim 32\%$ can be achieved [35]. The theoretical and experimental studies of effects of LSPR introduced by Au NPs on the optical and electrical properties of OSCs, particularly the OSC active layer will be discussed in this section.

8.3.1 Overall Device Performances

The absorption spectrum of PFSDCN film is shown in Fig. 8.8 and has two absorption peaks at around 374 and 518 nm. The chemical structure of PFSDCN is shown in the inset of Fig. 8.8. The optical bandgap and oxidation potential of PFSDCN are 2.05 eV and 0.91 V, respectively. The HOMO is -5.32 eV as measured by cyclic voltammetry (CV) method and the LUMO is -3.27 eV calculated from HOMO level and optical bandgap. The absorption spectrum of Au NPs in chloroform/chlorobenzene (1:1 v/v ratio) is shown in Fig. 8.9 with the peak at ~ 520 nm. The average diameter of Au NPs is ~ 18 nm determined from TEM measurement (inset of Fig. 8.9).

The J - V characteristics are shown in Fig. 8.10a. The effects of Au NPs concentration on performances including V_{OC} , J_{sc} , FF , and PCE of OSCs with structure of ITO/PEDOT:PSS (30 nm)/PFSDCN:PCBM (1:4 wt%; 2 mg/ml:8 mg/ml dissolved in chloroform/chlorobenzene (1:1, v/v ratio)): Au NPs/LiF (1 nm)/Al(100 nm) are shown in Fig. 8.10b (i)–(iv), respectively. It should be noted that the fabrication conditions such as the ratio of PFSDCN to PCBM, spin-coating

Fig. 8.8 The normalized absorption spectrum and chemical structure of PFSDCN [35]



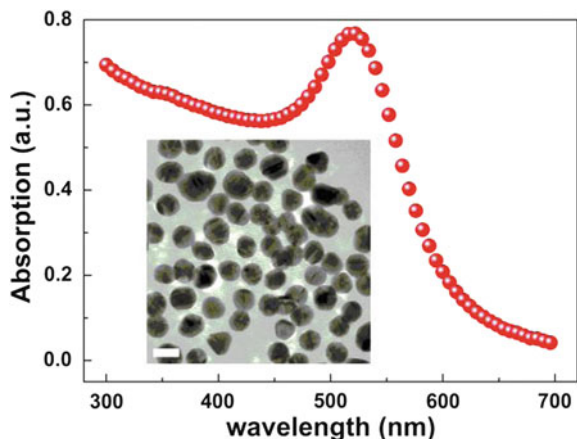


Fig. 8.9 The absorption spectrum of Au NPs in chloroform/chlorobenzene (1:1 volume ratio) with the peak at ~ 520 nm. *Inset* is the TEM image of Au NPs. The *white color bar* is 20 nm long [35]

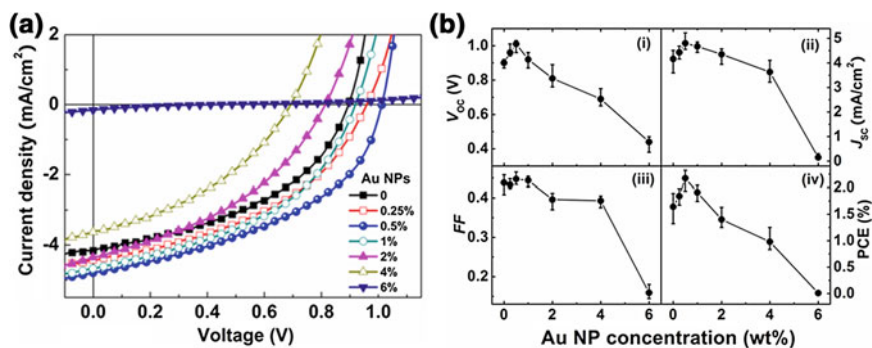


Fig. 8.10 **a** The current–voltage characteristics of the representative OSCs incorporated with different NP concentration under AM 1.5G illumination at 100 mW/cm^2 . **b** Electrical parameters of NP incorporated OSCs: (i) V_{OC} ; (ii) J_{sc} ; (iii) FF ; (iv) PCE [35]

speed and time, annealing temperature, and duration have been optimized for the control devices before the addition of Au NPs.

It is observed that Au NPs with a low concentration of 0.5 wt% improve V_{OC} and J_{sc} . However, both V_{OC} and J_{sc} reduce when Au NPs concentration increases further. FF increases slightly and then decreases as Au NPs concentration increases. From the dark J – V characteristic, it can be observed that the electrical conductivity improves by adding Au NPs, which is in good agreement with other reports [15]. However, the electrical conductivity reduces with the further increase of Au NPs concentration >2 wt%. Consequently, PCE is improved by $\sim 32\%$ from 1.64 (without Au NPs) to 2.17% (with 0.5 wt% Au NPs), and then

decreases. When Au NPs concentration reaches 6 wt%, almost no photovoltaic effect is observed (PCE \sim 0.01 %).

It should be noted that in the study [35], Au NPs have been capped with PEG. In order to investigate the effects of PEG on device performances, the PEG-only OSCs were fabricated in which only PEG was incorporated into the polymer blend. PEG concentration in the mixed solution is \sim 0.08 mg/ml which equals that of the PEG in 0.5 wt% Au NPs mixed with polymer blend solution. The PEG-only OSC shows similar J - V characteristics and PCE (\sim 1.67 %) to that of the device without PEG incorporation (PCE \sim 1.64 %). Therefore, PEG itself is not likely to have pronounced effects on device performances.

8.3.2 LSPR Effects

The degree of contributions of LSPR effect can be observed from the absorption spectrum of the active layer incorporated with various Au NPs concentrations, while the physical understanding can be obtained from theoretical analyzing the absorption of OSCs as shown in Fig. 8.11. The theoretical near-field profile of electric field (Fig. 8.11b) shows very strong field strength laterally distributed along the active layer which can enhance the light absorption by the polymer blend for generating carriers. It is noteworthy that when Au NPs incorporated into PEDOT:PSS layer (i.e., the layer adjacent to the active layer), the light absorption in the active layer is not clearly enhanced due to the lateral distribution feature of the strong LSPR near field along the PEDOT:PSS layer rather than a vertical distribution into the active layer as described in our another work [18].

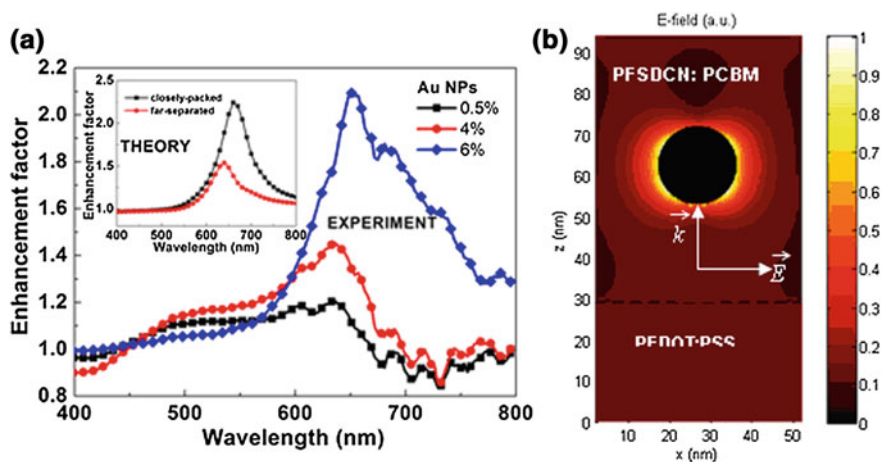
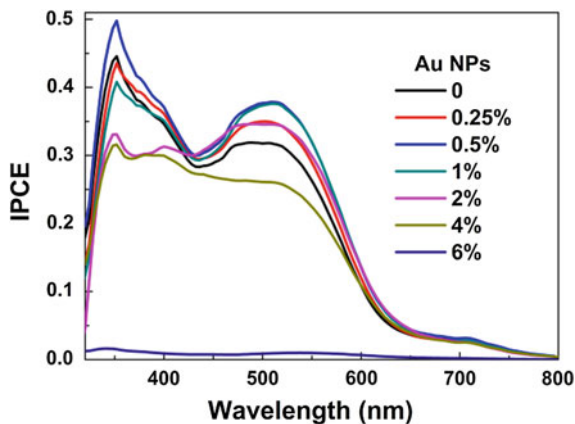


Fig. 8.11 **a** Experimental and theoretical (*inset*) absorbance enhancement factor of the active layer with different amount of Au NPs. **b** Theoretical near-field distribution around an Au NP in the active layer [35]

Fig. 8.12 IPCE of OSCs incorporated with different concentrations of Au NPs [35]



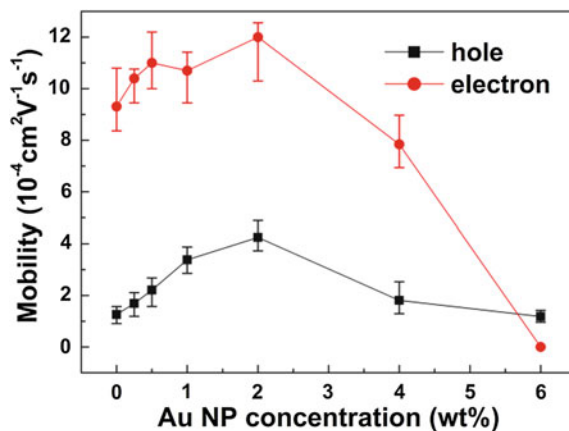
The theoretical and experimental absorption enhancement of the active layer (PFSDCN:PCBM) indicates that LSPR for the case of low Au NPs concentration mixed active layer exists at around 650 nm which is different from that of Au NPs (~ 520 nm) in chloroform/chlorobenzene (1:1 v/v ratio) due to the change of the surrounding optical environment. Moreover, when the spacing between Au NPs reduces (i.e., higher Au NPs concentration), the theoretical and experimental results show that the resonance strength increases and slightly red shifts. Consequently, the theoretical results are in agreement with the experimental results. The results demonstrate and explain the features of LSPR excited by Au NPs incorporated into OSCs active layer.

The light absorption can be enhanced experimentally by over 100 % at the resonance region when Au NPs concentration increases to 6 wt% as shown in Fig. 8.11a. However, the effects of LSPR alone cannot completely interpret the overall observed phenomena of OSCs. For example, low Au NPs concentration can benefit OSC performances. Continuously enhanced light absorption is obtained with the increase of Au NPs concentration due to the stronger LSPR. However, when Au NPs concentration >0.5 wt%, deterioration of device performances is obtained, which is quite unexpected in the viewpoint of LSPR effects. This can be further illustrated from IPCE characteristics as shown in Fig. 8.12. When the Au NPs concentration reaches 6 wt%, a large absorption enhancement factor is obtained (Fig. 8.11a), but IPCE decreases to almost zero. Therefore, besides LSPR effects, the effects of Au NPs on OSC electrical properties need to be investigated for understanding the results.

8.3.3 Effects on Carrier Mobility

Generally, electron and hole mobilities are the important factors and should be high enough to guarantee large carrier hopping rate, to avoid carrier recombination

Fig. 8.13 Effects of Au NP concentration on the hole and electron mobilities in the active layer [35]



and to prevent the build-up of space charge. [37, 38] For Au NPs incorporated OSCs, the hole and electron mobilities have been determined from hole-only and electron-only devices, respectively, by fitting from the dark J - V curves using the space-charge limited current (SCLC) model. [39] Hole-only devices have structures of ITO/PEDOT:PSS/polymer blend: Au NPs/Au (20 nm)/Al (80 nm). It has been reported that the work function of ITO can be effectively modified for electron collection in inverted OSCs by evaporating 1 nm of Ca [40, 41]. For our electron-only devices, the structure of ITO/Ca (2 nm)/polymer blend: Au NPs/LiF(1 nm)/Al(100 nm) has been investigated. The mobility of holes and electrons is shown in Fig. 8.13 and the detailed experimental data and fitting curves are shown in Fig. 8.14. The hole mobility (1.18 – $4.25 \times 10^{-4} \text{ cm}^2 \text{ V}^{-1} \text{ s}^{-1}$) is about one order less than electron mobility (0.78 – $1.2 \times 10^{-3} \text{ cm}^2 \text{ V}^{-1} \text{ s}^{-1}$) except for that of OSC with 6 wt% Au NPs. Hence, the charge transport of the devices is dominantly limited by the hole transport property, which agrees well with the fact that the transport process in the organic materials is dominated by the slow charge carriers [42].

The effects of Au NPs on the carrier mobility are manifold. On the one hand, Au NPs can introduce dopant states within the bandgap of polymer which can provide hopping sites for holes, and thus enhance the mobility [15]. In fact, the metallic NP-induced energy levels for holes have also been reported previously in a hybrid Ag NPs/organic resonant tunneling diode [43]. On the other hand, the incorporated Au NPs will modify the nanoscale morphology of the polymer/fullerene blend, especially with high NPs concentration, which can be evidenced by the AFM image as shown in Fig. 8.15. The root mean square (RMS) roughness of the active layer increases significantly from ~ 0.617 (without Au NPs) to ~ 8.062 nm (6 wt% Au NPs) and an obvious different surface morphology is observed. In addition, the phase image shows a much larger contrast for the active layer film with 6 wt% Au NPs, indicating a nanoscale morphology change of the blends. [44, 45] Such NPs-induced nanoscale morphology change may not favor charge transport, and thus degrades the carrier mobility. The two factors will

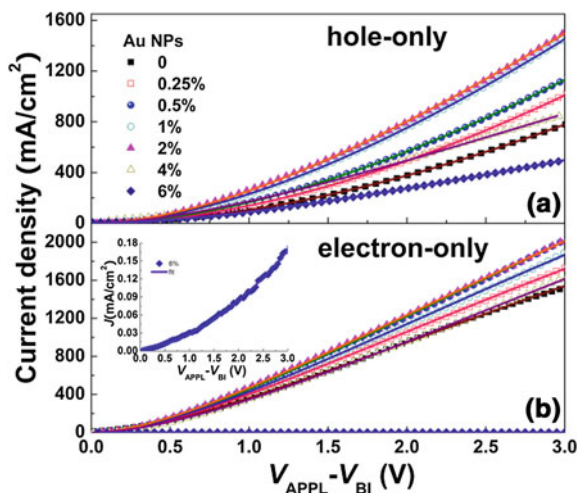


Fig. 8.14 Experimental data (*symbols*) and fitted J - V curves (*solid lines*) of a hole-only devices **b** electron-only devices. The electrical conductivity of electron-only device with 6 wt% Au NP concentration is rather low, and thus is shown in the *inset* of (b) [35]

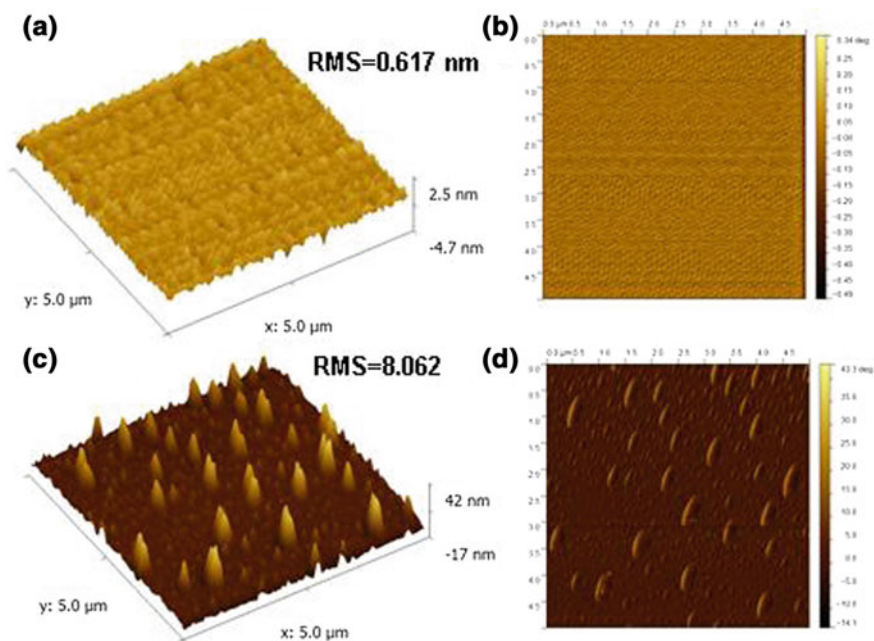
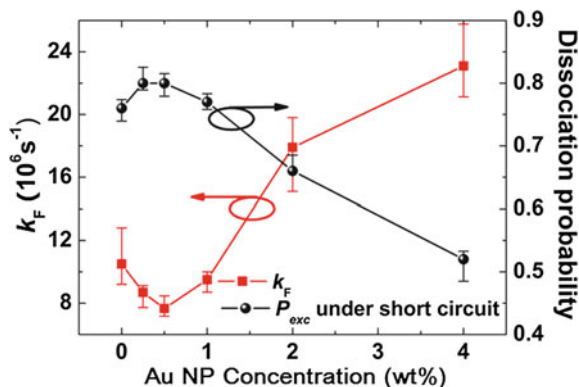


Fig. 8.15 AFM images of the active layer **a** height image, RMS = 0.617 nm and **b** phase image of active layer film without Au NPs; **c** height image, RMS = 8.062 nm and **d** phase image of active layer film with Au NPs: 6 wt% [35]

Fig. 8.16 Effects of Au NP concentration on the decay rate of bound electron–hole pair (k_F) (square) and exciton dissociation probability (P_{exc}) under short-circuit condition (circle) [35]



therefore compete with each other in our devices. At low Au NPs concentration, the blend morphology does not have clear changes from our AFM results (i.e., rms. roughness only increases to ~ 1.204 nm for 1 wt% Au NP incorporation, and therefore only plays a less important role in modifying carrier mobility. As a result, with low Au NPs concentration, the increases of carrier mobility should be explained by the introduction of hopping sites for holes. These hopping sites are expected to have greater influence on hole mobility than electron mobility, which agrees well with the experimental results. Compared with the control devices (without Au NPs), incorporation with 2 wt% Au NPs contributes to an improvement of hole mobility by $\sim 237\%$ (from 1.26×10^{-4} to $4.25 \times 10^{-4} \text{ cm}^2 \text{ V}^{-1} \text{ s}^{-1}$), and an improvement of electron mobility only by $\sim 28\%$ (from 0.93×10^{-3} to $1.2 \times 10^{-3} \text{ cm}^2 \text{ V}^{-1} \text{ s}^{-1}$). With high Au NPs concentration, the NP-induced morphology change dominates the charge transport process, and thus both the hole and electron mobility are expected to degrade, which is well consistent with the experimental results as shown in Fig. 8.16. Therefore, the enhanced carrier mobilities with the proper amount of Au NPs can partly account for the improved photocurrent generation and FF due to the improved carrier collection and the reduced bulk resistance. However, when the carrier mobility maintains increment until Au NPs concentration reaching 2 wt%, device performances, i.e., J_{sc} and PCE decrease when Au NPs concentration ≥ 1 wt%. This indicates that besides the carrier mobility, Au NPs should affect other operation processes of OSCs. One process likely to be affected is the dissociation of excitons to free carriers as described below.

8.3.4 Effects on Exciton Dissociation

The efficiency of exciton dissociation can be investigated by fitting photocurrent (J_{ph}) as a function of effective voltage (V_{EFF}) as reported in Mihailetchi et al. [46]. The maximal generation rate of excitons (G_{max}) for all the devices with different

Au NPs concentration [35] is on the order of $5 \times 10^{27} \text{ m}^{-3} \text{ s}^{-1}$. The exciton decay rate (k_F) and exciton dissociation probability (P_{exc}) under short-circuit condition are shown in Fig. 8.16. It can be observed that Au NPs indeed affects the exciton dissociation. Low Au NPs concentration makes k_F reduce and P_{exc} increase slightly from ~ 76 to ~ 80 %. While Au NPs concentration further increases, P_{exc} reduces.

The slight enhancement of P_{exc} at low Au NPs concentration can be attributed to the excitation of LSPR [47] and the enhanced hole mobility which reduces the carrier back-transfer induced recombination. [37, 42] The degradation of exciton dissociation efficiency at high NPs concentration can be attributed to the morphology change of the active layer and the reduced V_{OC} . As indicated from the surface image of the active layer in Fig. 8.15, the nanoscale morphology change inside the active layer is significant especially at high NPs concentration. Such NP-induced morphology change may make the polymer blend less favorable for exciton dissociation. On the other hand, the reduction of V_{OC} means a decrease of built-in electric field in the active layer, which will make the exciton dissociation process less efficient since the exciton dissociation is very field-dependent [48].

8.3.5 V_{oc}

As Au NPs concentration increases, V_{OC} first increases from ~ 0.90 (without Au NPs) to ~ 1.01 V (Au NPs: 0.5 wt%) and then decreases. When Au NPs concentration increases to 6 wt%, V_{OC} reduces significantly to 0.44 V. In BHJ OSCs, charge recombination is commonly regarded as one important loss mechanism limiting V_{OC} . [49, 50]. With a proper amount of Au NPs (≤ 0.5 %), the reduced recombination due to the enhanced carrier mobility and exciton dissociation is expected to improve V_{OC} . Theoretical studies built based on the fundamental equations describing carrier transports in semiconductors following Koster et al. [42] have been conducted to understand the contribution of recombination reduction on V_{OC} . Details of the model can be found in Appendix A. In modeling, the device parameters for OSCs with various Au NPs such as carrier mobilities and k_F are obtained by experiment and modeling in the previous sections, while other parameters are remained constant. The results show that V_{OC} has almost no change, suggesting that the reduced recombination due to increased carrier mobilities does not contribute to the V_{OC} improvement. An alternative explanation for the V_{OC} improvement with Au NPs incorporation (≤ 0.5 wt%) is the downwards shift of the donor HOMO level due to reduced polarization energy [51, 52]. Downwards shift of donor HOMO level by 0.1 eV is best fitted as shown in Appendix A: Fig. 8.17, for the increase of the measured V_{OC} by ~ 0.1 V for 0.5 wt% Au NP case.

The degradation of V_{OC} at high Au NPs concentration is due to several factors. At high concentration, large amount of Au NPs may modify the interfacial charge states at the cathode and even breakdown the Fermi level pinning between the

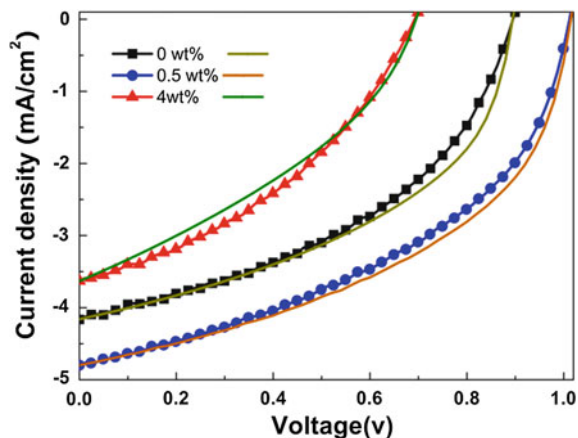


Fig. 8.17 J - V characteristics of the OSCs with different Au NPs concentration under AM 1.5G illumination at 100 mW/cm^2 . The symbols denote experimental data (squares: without Au NPs; circles: Au NPs 0.5 wt%; triangles: Au NPs 4 wt%). The solid lines denote theoretical results [35]

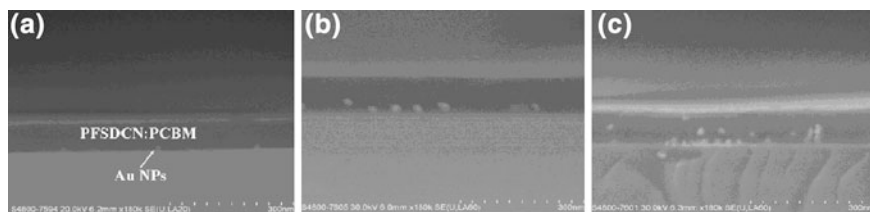


Fig. 8.18 SEM cross-section image of the active layer embedding with Au NPs **a** 0.5 wt%, **b** 2 wt% and **c** 6 wt% [35]

cathode metal and the fullerene reduction potential, which can downward shift the cathode work function and lead to remarkable V_{OC} reduction. This can be further revealed by the SEM cross-section images of the active layer in Fig. 8.18. With low concentration of Au NPs (0.5 and 2 wt%), the Au NPs are mostly located near the bottom of PFSDCN:PCBM (near to the interface with PEDOT:PSS). When embedding high concentration Au NPs (6 wt%, Fig. 8.18c), aggregation of NPs is observed and some are located at the surface of the active layer, which induce a significant morphology change and V_{OC} reduction. The theoretical results show that the change of work function of the cathode causes the reduction of V_{OC} . When the cathode work function is downward shifting by 0.56 eV, V_{OC} reduces to 0.69 V for OSCs with 4 wt% of Au NPs concentration. The other subordinate factor resulting in V_{OC} reduction is that more shunt paths are induced by the Au NPs, which can be well indicated from the increased reverse current for the OSCs as the concentration of Au NPs increases. The shunt paths formed directly from anode to cathode are believed to reduce the V_{OC} [53, 54].

8.3.6 Section Summary

The effects of Au NPs incorporated into the active layer PFSDCN:PCBM of OSCs have been described in this section. Theoretical simulations indicated that the near field of NPs distribute laterally along the active layer, leading to the absorption improvement which is also experimentally observed. On the other hand, electrical properties of these OSCs are also described. The carrier mobility is found to increase upon incorporation of NPs. In particular, hole mobility increased to a larger extent than electron mobility, leading to reduced carrier transport imbalance. Exciton dissociation efficiency is found to increase then decrease as NP concentration is increased. The active layer morphology is also altered after NP incorporation. These factors together lead to the observed PCE trend.

8.4 Efficiency Improvement of Polymer Solar Cells by Incorporating Au Nanoparticles into All Polymer Layers

Although PCE of OSCs has been shown to improve by incorporating metallic NPs in either the buffer layer such as PEDOT:PSS or the active layer [6, 7, 9–11, 47, 55], we have shown in Sects. 8.2 and 8.3 that in fact, the contribution of LSPR effects to PCE improvements varies when NPs are doped in different layers. Electrical properties such as carrier mobility, exciton dissociation probability, and the morphology of the organic layer incorporated with NPs are affected by NPs, and are major contributors to the PCE changes as NP concentration increases. With the experience of incorporating NPs individually in the hole collection layer or active layer, we noticed that there are very limited studies on incorporating metallic NPs in more than one organic layer. The study of incorporation of NPs in all organic layers has two objectives: (1) Achieving high efficiency OSCs by incorporating NPs within all possible layers of a OSC; (2) Investigating their effects on the optical and electrical properties, in particular, observing the presence of interaction between the NPs in different layers, if any. Achieving these two objectives will enhance our understanding in device mechanisms and is essential for designing high efficiency NP-incorporated OSCs.

In this work, monofunctional PEG-capped Au NPs of sizes 18 and 35 nm are doped in the PEDOT:PSS and P3HT:PCBM layers, respectively, leading to an improvement of PCE by $\sim 22\%$ compared to the optimized control device. We will first identify the impact of NPs in each polymer layer on OSC characteristics by doping Au NPs in either the PEDOT:PSS or P3HT:PCBM layer. Then, we will investigate the impact of Au NPs incorporated in all polymer layers. We demonstrate that the accumulated benefits of incorporating Au NPs in all organic layers of OSCs can achieve larger improvements in OSC performances.

8.4.1 Performances of Au NP Devices

Four device structures have been investigated [56] as follows:

Device A: (control): ITO/PEDOT:PSS/P3HT:PCBM/LiF (1 nm)/Al (100 nm)

Device B: ITO/PEDOT:PSS + Au NPs/P3HT:PCBM/LiF (1 nm)/Al (100 nm)

Device C: ITO/PEDOT:PSS/P3HT:PCBM + Au NPs/LiF (1 nm)/Al (100 nm)

Device D: ITO/PEDOT:PSS + AuNPs/P3HT:PCBM + Au NPs/LiF (1 nm)/Al (100 nm)

J - V characteristics of the four OSC device structures with Au NPs incorporated into different organic layers are shown in Fig. 8.19, and the photovoltaic parameters are listed in Table 8.2.

We observe that the incorporation of Au NPs into either the PEDOT:PSS layer (Device B) or the active layer (Device C) or improves PCE from 3.16 (control Device A) to 3.61 and 3.44 %, respectively. Interestingly, the simultaneous incorporation of Au NPs into both layers results in a further improvement of average PCE to 3.85 %, which corresponds to ~ 22 % increment from the control Device A. In all cases, the increases in PCE are results of improvements in J_{sc} and FF , while the V_{OC} is unchanged. Notably, when incorporating Au NPs into both PEDOT:PSS and active layer simultaneously, the series resistance (R_s) reduces obviously from 3.05 (Device A) to 1.93 $\Omega\cdot\text{cm}^2$ (Device D), contributing to a remarkable increase of FF from 61.92 to 65.00 %. To study the origins of PCE improvement, we first separately study the effects of NPs when incorporated into either the PEDOT:PSS or P3HT:PCBM layer, which is followed by discussions on PCE improvement when NPs are incorporated in all polymer layers.

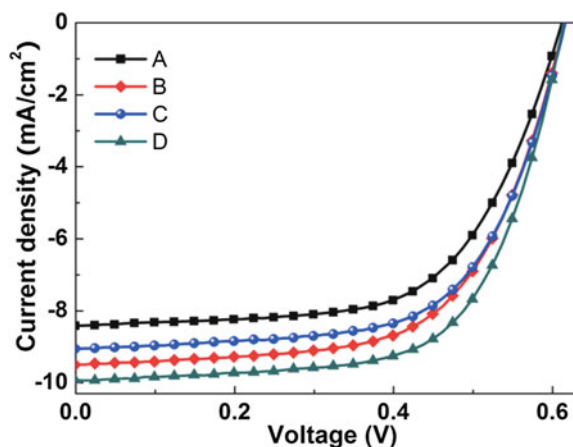


Fig. 8.19 a J - V characteristics of the OSCs with NPs incorporated into different layers under AM 1.5G illumination at 100 mW/cm^2 [35]

Table 8.2 Photovoltaic parameters of the PSCs with NPs incorporated in different layers under AM 1.5G illumination at 100 mW/cm^2 . R_S is derived from the slope of the current–voltage (J – V) curves under dark at 2 V [56]

Device	V_{OC} (V)	J_{sc} (mA/cm^2)	FF (%)	PCE (%)	R_S ($\Omega\cdot\text{cm}^2$)
A	0.61 ± 0.00	8.35 ± 0.09	61.92 ± 0.33	3.16 ± 0.04	3.05 ± 0.03
B	0.61 ± 0.01	9.41 ± 0.28	62.52 ± 0.66	3.61 ± 0.08	2.11 ± 0.06
C	0.61 ± 0.00	8.85 ± 0.27	63.56 ± 0.53	3.41 ± 0.11	2.92 ± 0.13
D	0.61 ± 0.01	9.74 ± 0.57	65.00 ± 1.02	3.85 ± 0.20	1.93 ± 0.04

8.4.2 Effects of Au NPs Incorporated in the PEDOT:PSS Layer Only

For the case of Au NPs doped into the PEDOT:PSS layer only (Device B), a study of the physics been conducted in Sect. 8.2 [18]. In this set of experiment, the absorption spectrum of the active layer does not show any clear change from the control Device A as shown in Fig. 8.20.

This is in good agreement with previous report [18], which can be explained by the finding that the strong near field around Au NPs due to the LSPR distributes laterally along the PEDOT:PSS layer instead of vertically penetrating into the active layer. Meanwhile, from the hole mobilities of Devices A and B derived from the hole-only devices, there is no obvious changes (see Fig. 8.21), indicating that charge transport in the bulk of the active layer is unaffected by NPs incorporated in PEDOT:PSS. The surface morphology of the PEDOT:PSS + Au NPs layer showed an obvious increase in surface roughness with the RMS roughness increasing from 0.97 to 1.55 nm. Therefore, the incorporation of Au NPs only in PEDOT:PSS increases the interfacial contact area between the active layer (P3HT:PCBM) and PEDOT:PSS, allowing more efficient hole collection at the anode, and hence increases J_{sc} and FF [23, 57]. Furthermore, from resistive

Fig. 8.20 Absorbance of the active layer for different NP doping structures [56]

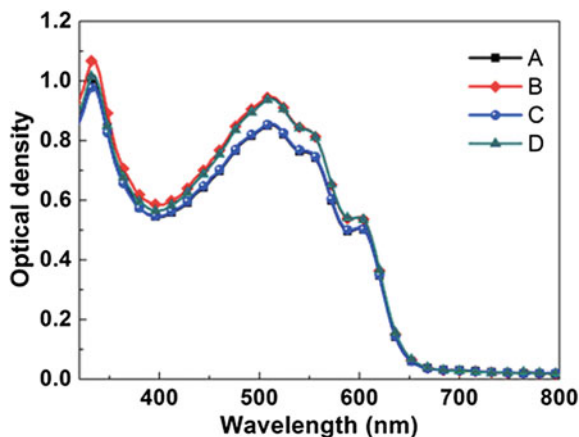
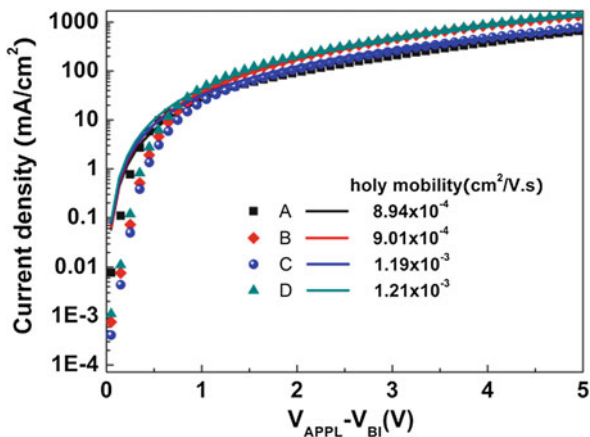


Fig. 8.21 The J - V characteristics of hole-only devices with Au NPs incorporated into different layers with the structure of ITO/PEDOT:PSS (with or without Au NPs)/P3HT:PCBM (with or without Au NPs)/Au (20 nm)/Al (100 nm). The symbols are experimental data while the lines are fitting curves. Fitting is done according to the space-charge limited current model [56]



devices of structure ITO/PEDOT:PSS (with or without Au NPs)/Al, it is found that the resistance of PEDOT:PSS reduces upon addition of NPs. Both the increased interfacial contact area and conductivity of PEDOT:PSS contributes to the reduction of the series resistance of OSCs from 3.05 to 2.11 $\Omega \cdot \text{cm}^2$, and improvement of FF and PCE .

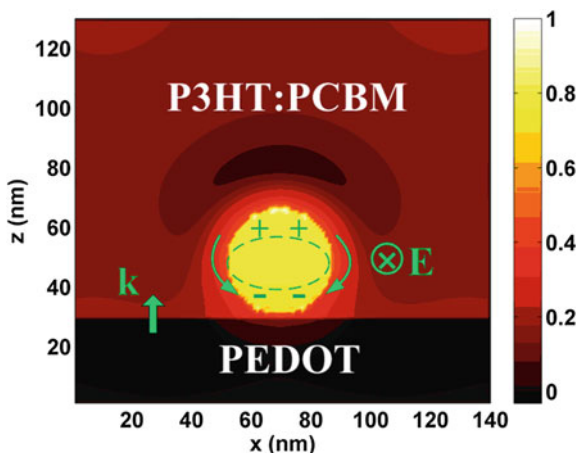
8.4.3 Effects of Au NPs Incorporated into P3HT:PCBM

Although electrical effects dominantly address the performance improvement when incorporating Au NPs only in PEDOT:PSS, the mechanism for PCE improvement is found to be different when NPs are incorporated into the active layer. In contrast to Sect. 8.3, a different active layer material, P3HT:PCBM is used instead of PFSDCN:PCBM and the device characteristics are investigated here. As shown in Fig. 8.20, when NPs are incorporated into the active layer only (Device C), absorption of the active layer increases over a wide wavelength range.

From the theoretical studies [56], it is found that the absorption enhancement can be explained by LSPRs in the Au NPs excited by the TE polarized light. The dipoles generated in the Au NPs and the strong near field by LSPRs by Au NPs in the active layer are shown in Fig. 8.22. It can be observed that the strong near field distributes into the active layer and directly enhance the light absorption by the blended polymers of the active layer.

As a result of the strong near field of NPs which overlaps with the active layer, the amount of photogenerated excitons is increased, and hence increases the J_{sc} of OSCs. Regarding electrical properties, J - V measurements and fitting on hole-only devices indicate that the hole mobility of the active layer increases from 8.94×10^{-4} to 1.19×10^{-3} $\text{cm}^2/\text{V}\cdot\text{s}$. Studies have shown that in P3HT:PCBM, electron mobility is higher than hole mobility and this carrier imbalance is

Fig. 8.22 The schematic pattern for the plasmon resonance and charge distribution of an Au NP, as well as the near-field distributions for the vertically incident light with TE polarization in P3HT:PCBM [56]

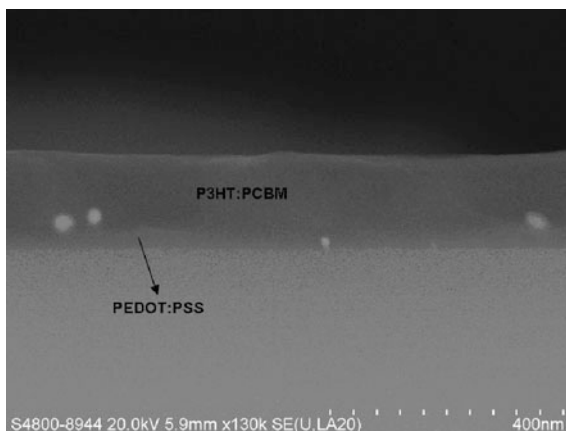


detrimental to the photovoltaic performance [29]. The increase in hole mobility allows more balanced charge transport in the active layer, thus improving the J_{sc} and FF of the device.

8.4.4 Effects of Au NPs Incorporated in All Polymer Layers

When Au NPs are doped into both PEDOT:PSS and the active layer, the PCE of our OSCs further increases to 3.85 %. From hole-only devices, the hole mobility of P3HT:PCBM is determined to be $\sim 1.21 \times 10^{-3} \text{ cm}^2/\text{V.s}$, which is similar to the case when NP is doped in the active layer only ($1.19 \times 10^{-3} \text{ cm}^2/\text{V.s}$). From the cross-section SEM images are shown in Fig. 8.23, Au NPs doped in the active layer are mostly located at the bottom of P3HT:PCBM (near to the interface with PEDOT:PSS), while the Au NPs doped to PEDOT:PSS are well embedded in the PEDOT:PSS layer. However, despite the fact that the active layer is adjacent to the PEDOT:PSS layer, the highly similar absorption spectra of Devices C (Au NPs in P3HT:PCBM only) and D (Au NPs in both P3HT:PCBM and PEDOT:PSS) shown in Fig. 8.20 show that there is no clear interaction between the Au NPs in the active layer and those in the PEDOT:PSS layer. From the principle of optics, the absence of couplings between Au NPs in PEDOT and Au NPs in P3HT:PCBM is reasonable, because the polarization direction of the electric field of vertically incident light is parallel to each device layer. Furthermore, we have shown that the improvement mechanisms when incorporating NPs in PEDOT:PSS mainly originates from PEDOT:PSS/P3HT:PCBM interfacial effects, while incorporating NPs in the active layer mainly improves optical absorption and charge transport in the bulk of the active layer. As interfacial and bulk effects are two individual effects and optical coupling between NPs is not observed, we expect that the improvement of PCE from 3.16 to 3.85 % is the accumulated improvements of addition of NPs into the individual layers.

Fig. 8.23 Representative cross-section SEM image of the film structure PEDOT:PSS + Au NPs/P3HT:PCBM + Au NPs [35]



8.4.5 Section Summary

In conclusion, by incorporating Au NPs into all organic layers in the OSCs, the efficiency can be improved by 22 %. The improvement is attributed to the accumulated enhancements in device performance due to addition of NPs into individual layers. NPs doped into PEDOT:PSS mainly contributes to more efficient hole collection due to increased PEDOT:PSS/P3HT:PCBM interfacial area, while NPs doped into the active layer improves optical absorption by LSPR effects and improves the hole mobility of the active layer. No optical coupling was observed between NPs in PEDOT:PSS and P3HT:PCBM. As the effects of NPs in PEDOT:PSS or P3HT:PCBM are separated, the PCE improvement was attributed to the accumulated benefits of NPs in the individual organic layers. Although the NPs in different layer did not interact to achieve extra improvements in PCE, this study shows that the advantages of incorporating NPs in individual layers can be utilized together to achieve larger increases of OSC performance and the role of NPs play when incorporated into OSCs has been further clarified, which is highly useful in designing high efficiency OSCs in the future.

8.5 Conclusions

We have discussed in detail that the effect of incorporation of NPs into various layers of an OSC. In Sect. 8.2, it has been reported [36] that about 13 % improvement in PCE for PSCs incorporating PEG-capped Au NPs in PEDOT:PSS, with enhancements mainly originating from J_{sc} and FF. A peak in PCE performance is obtained at an Au NP concentration of 0.32 wt% [35]. The contribution of LSPR effect to performance improvement has been theoretically and experimentally described. Both theoretical and experimental results show that absorption

enhancement due to incorporation of Au NPs is insignificant and provides only minor contribution to PCE improvement. It is found that the reason is due to the lateral distribution feature of the strong near-field of plasmonic resonance around the metallic NPs. Importantly, the finding can also be applied to other cases with metallic NPs (such as Ag and Pt) incorporated into the buffer layer adjacent to active layers of typical organic thin film solar cells. These studies [35, 58], that the optical properties of OSCs such as the direction dependence of absorption enhancement cannot but fully described by traditional physical quantities, such as scattering cross-section. It is highly necessary to account for near-field physics in order to provide a full picture for the effective optical design of photovoltaics.

Considering electrical characteristics, it is found [18] that the incorporation of an appropriate amount of Au NPs reduces the resistance of PEDOT:PSS layer. AFM images of NP incorporated PEDOT:PSS show that there is an increase in the interfacial roughness between P3HT:PCBM and PEDOT:PSS after incorporation of Au NPs. The roughened interface contributes to the improvement of hole collection efficiency and leads to J_{sc} and FF enhancements. PL measurements show that incorporation of Au NPs lead to reduced exciton quenching at D/A junctions at high NP concentrations due to change in internal networking of the active layer. The report indicates [18] that the competition between the effects of hole collection improvements and reduced exciton quenching, instead of LSPR effects, lead to the performance peak at 0.32 wt%.

In Sect. 8.3, the effects of PEG-capped Au NPs (0.5 wt%) on OSCs have been theoretically and experimentally discussed by introducing the Au NPs into a blend of a newly synthesized polymer of PFSDCN and PCBM [35]. The results show that due to the interesting feature of the strong lateral distribution of LSPR near field along the active layer, light absorption is enhanced by incorporating Au NPs into the active layer. This is in stark contrast with the case of NPs incorporated into PEDOT:PSS where LSPR cannot contribute to absorption enhancement.

Meanwhile, our discussion shows that electrical properties are also strongly affected by the NPs. Carrier mobility was found to increase which is beneficial to device performance. In particular, hole mobility increases at a quicker rate than electron mobility which may contribute to reducing carrier mobility imbalance. Exciton dissociation probability is also found to increase slightly then decrease rapidly upon increasing NP concentration. The morphology of the active layer is also strongly altered by high concentrations of Au NPs. The interplay of these various factors showed that enhancement in electrical properties can initially improve OSC performance at low NP concentrations. At higher concentrations, electrical effects can counter-diminish the optical enhancement from LSPR which reduces the overall performance improvement. Hence, it is very important that both optical and electrical properties need to be studied and optimized simultaneously. After optimization, power conversion efficiency can be improved by $\sim 32\%$ [35].

The studies in Sects. 8.2 and 8.3 have provided us with insights into the device mechanisms of OSCs. The role of LSPR is found to be not as important as many studies claimed to be in improving PCE of solar cells. In particular, only NPs

incorporated in the active layer can utilize LSPR to improve active layer absorption. On the other hand, electrical properties are found to play significant roles in improving PCE. Our studies highlight the important point that both electrical and optical characteristics have to be investigated in OSCs, and our findings are highly useful in the design of NP-incorporated solar cells.

In Sect. 8.4, Au NPs incorporated into both the hole collection layer and the active layer have been discussed. A large increase in PCE ($\sim 22\%$) has been reported [56] which is attributed to the stacked improvements of NPs incorporating in the hole collection layer and the active layer. Coupling is not observed between NPs in the different layers, but this study shows that NPs can be incorporated in all layers to achieve large improvements in efficiency.

Appendix A

The electrical properties of OSCs with Au NPs in the active layer of PFSDCN:PCBM [35] have been theoretically studied by solving the organic semiconductor equations involving Poisson, drift–diffusion, and continuity equations [42, 46, 59]. The field-dependent mobility uses the Frenkel-Poole form $\mu = \mu_0 \cdot \exp(F/F_0)$. The Braun-Onsager model is employed for the exciton dissociation. The boundary conditions for ohmic or schottky contacts are also taken into account.

Due to the very thin active layer (~ 65 nm), it can be assumed the generation rate of bound electron–hole pairs (G_{max}) is uniform. G_{max} can be obtained from the measured absorption spectra. The electron and hole mobilities can be obtained by fitting the J – V curves of the measured electron- and hole-only devices following the SCLC model. The HOMO is -5.32 eV as measured by cyclic voltammetry (CV) method and the LUMO is -3.27 eV calculated from HOMO level and optical bandgap. The exciton decay rate (k_F) of exciton and charge separation distance (a) can be fitted to make our theoretical J – V curves best fit to the experimental J – V curves

References

1. Anker JN, Hall WP, Lyandres O, Shah NC, Zhao J, Van Duyne RP (2008) Biosensing with plasmonic nanosensors. *Nat Mater* 7(6):442–453
2. Stockman MI (2004) Nanofocusing of optical energy in tapered plasmonic waveguides. *Phys Rev Lett* 93(13):137404
3. Shalaev VM (2007) Optical negative-index metamaterials. *Nat Photon* 1(1):41–48
4. Chang DE, Sorensen AS, Demler EA, Lukin MD (2007) A single-photon transistor using nanoscale surface plasmons. *Nat Phys* 3(11):807–812
5. Atwater HA, Polman A (2010) Plasmonics for improved photovoltaic devices. *Nat Mater* 9(3):205–213

6. Chen F-C, Wu J-L, Lee C-L, Hong Y, Kuo C-H, Huang MH (2009) Plasmonic-enhanced polymer photovoltaic devices incorporating solution-processable metal nanoparticles. *Appl Phys Lett* 95(1):013305
7. Wu J-L, Chen F-C, Hsiao Y-S, Chien F-C, Chen P, Kuo C-H, Huang MH, Hsu C-S (2011) Surface plasmonic effects of metallic nanoparticles on the performance of polymer bulk heterojunction solar cells. *ACS Nano* 5(2):959–967. doi:[10.1021/nn102295p](https://doi.org/10.1021/nn102295p)
8. Morfa AJ (2008) Plasmon-enhanced solar energy conversion in organic bulk heterojunction photovoltaics. *Appl Phys Lett* 92(1):013504
9. Kim S (2008) Plasmon enhanced performance of organic solar cells using electrodeposited Ag nanoparticles. *Appl Phys Lett* 93(7):073307
10. Wang DH, Kim DY, Choi KW, Seo JH, Im SH, Park JH, Park OO, Heeger AJ (2011) Enhancement of donor–acceptor polymer bulk Heterojunction solar cell power conversion efficiencies by addition of Au nanoparticles. *Angew Chem Int Ed* 50(24):5519–5523. doi:[10.1002/anie.201101021](https://doi.org/10.1002/anie.201101021)
11. Kim C-H, Cha S-H, Kim SC, Song M, Lee J, Shin WS, Moon S-J, Bahng JH, Kotov NA, Jin S-H (2011) Silver nanowire embedded in P3HT:PCBM for high-efficiency hybrid photovoltaic device applications. *ACS Nano* 5(4):3319–3325. doi:[10.1021/mn200469d](https://doi.org/10.1021/mn200469d)
12. Naidu BVK, Park JS, Kim SC, Park S-M, Lee E-J, Yoon K-J, Joon Lee S, Wook Lee J, Gal Y-S, Jin S-H (2008) Novel hybrid polymer photovoltaics made by generating silver nanoparticles in polymer: fullerene bulk-heterojunction structures. *Sol Energy Mater Sol Cells* 92(4):397–401. doi:[10.1016/j.solmat.2007.09.017](https://doi.org/10.1016/j.solmat.2007.09.017)
13. Min C (2010) Enhancement of optical absorption in thin-film organic solar cells through the excitation of plasmonic modes in metallic gratings. *Appl Phys Lett* 96(13):133302
14. Kang M-G, Xu T, Park HJ, Luo X, Guo LJ (2010) Efficiency enhancement of organic solar cells using transparent plasmonic Ag nanowire electrodes. *Adv Mater* 22(39):4378–4383. doi:[10.1002/adma.201001395](https://doi.org/10.1002/adma.201001395)
15. Kim K, Carroll DL (2005) Roles of Au and Ag nanoparticles in efficiency enhancement of poly(3-octylthiophene)/C[₆₀] bulk heterojunction photovoltaic devices. *Appl Phys Lett* 87(20):203113
16. Sha WEI, Choy WCH, Liu YG, Cho Chew W (2011) Near-field multiple scattering effects of plasmonic nanospheres embedded into thin-film organic solar cells. *Appl Phys Lett* 99(11):113304
17. Enüstün BV, Turkevich J (1963) Coagulation of colloidal gold. *J Am Chem Soc* 85(21):3317–3328. doi:[10.1021/ja00904a001](https://doi.org/10.1021/ja00904a001)
18. Fung DDS, Qiao L, Choy WCH, Wang C, Sha WEI, Xie F, He S (2011) Optical and electrical properties of efficiency enhanced polymer solar cells with Au nanoparticles in a PEDOT-PSS layer. *J Mater Chem* 21(41):16349–16356
19. Bouyer F, Robben A, Yu WL, Borkovec M (2001) Aggregation of colloidal particles in the presence of oppositely charged polyelectrolytes: effect of surface charge heterogeneities. *Langmuir* 17(17):5225–5231. doi:[10.1021/la010548z](https://doi.org/10.1021/la010548z)
20. Qian J, Jiang L, Cai F, Wang D, He S (2011) Fluorescence-surface enhanced Raman scattering co-functionalized gold nanorods as near-infrared probes for purely optical in vivo imaging. *Biomaterials* 32(6):1601–1610. doi:[10.1016/j.biomaterials.2010.10.058](https://doi.org/10.1016/j.biomaterials.2010.10.058)
21. Catchpole KR, Polman A (2008) Design principles for particle plasmon enhanced solar cells. *Appl Phys Lett* 93(19):191113
22. Lee J-Y, Peumans P (2010) The origin of enhanced optical absorption in solar cells with metal nanoparticles embedded in the active layer. *Opt Express* 18(10):10078–10087
23. Hsu M-H, Yu P, Huang J-H, Chang C-H, Wu C-W, Cheng Y-C, Chu C-W (2011) Balanced carrier transport in organic solar cells employing embedded indium-tin-oxide nanoelectrodes. *Appl Phys Lett* 98(7):073308
24. Li G, Shrotriya V, Yao Y, Yang Y (2005) Investigation of annealing effects and film thickness dependence of polymer solar cells based on poly(3-hexylthiophene). *J Appl Phys* 98(4):043704

25. Chen L-M, Xu Z, Hong Z, Yang Y (2010) Interface investigation and engineering—achieving high performance polymer photovoltaic devices. *J Mater Chem* 20(13):2575–2598
26. Becker H, Burns SE, Friend RH (1997) Effect of metal films on the photoluminescence and electroluminescence of conjugated polymers. *Phys Rev B* 56(4):1893
27. Markov DE, Blom PWM (2005) Migration-assisted energy transfer at conjugated polymer/metal interfaces. *Phys Rev B* 72(16):161401
28. Zhokhavets U, Erb T, Hoppe H, Gobsch G, Serdar Sariciftci N (2006) Effect of annealing of poly(3-hexylthiophene)/fullerene bulk heterojunction composites on structural and optical properties. *Thin Solid Films* 496(2):679–682. doi:[10.1016/j.tsf.2005.09.093](https://doi.org/10.1016/j.tsf.2005.09.093)
29. Li G, Shrotriya V, Yao Y, Huang J, Yang Y (2007) Manipulating regioregular poly(3-hexylthiophene): [6]-phenyl-C61-butyric acid methyl ester blends-route towards high efficiency polymer solar cells. *J Mater Chem* 17(30):3126–3140
30. Shen H, Bienstman P, Maes B (2009) Plasmonic absorption enhancement in organic solar cells with thin active layers. *J Appl Phys* 106(7):073109
31. Drees M, Hoppe H, Winder C, Neugebauer H, Sariciftci NS, Schwinger W, Schaffler F, Topf C, Scharber MC, Zhu Z, Gaudiana R (2005) Stabilization of the nanomorphology of polymer-fullerene “bulk heterojunction” blends using a novel polymerizable fullerene derivative. *J Mater Chem* 15(48):5158–5163
32. Kim Y, Cook S, Tuladhar SM, Choulis SA, Nelson J, Durrant JR, Bradley DDC, Giles M, McCulloch I, Ha C-S, Ree M (2006) A strong regioregularity effect in self-organizing conjugated polymer films and high-efficiency polythiophene: fullerene solar cells. *Nat Mater* 5(3):197–203
33. Kim H, So W-W, Moon S-J (2007) The importance of post-annealing process in the device performance of poly(3-hexylthiophene): Methanofullerene polymer solar cell. *Sol Energy Mater Sol Cells* 91(7):581–587. doi:[10.1016/j.solmat.2006.11.010](https://doi.org/10.1016/j.solmat.2006.11.010)
34. Topp K, Borchert H, Johnen F, Tunc AV, Knipper M, von Hauff E, Parisi J, Al-Shamery K (2009) Impact of the incorporation of Au nanoparticles into polymer/fullerene solar cells†. *J Phys Chem A* 114(11):3981–3989. doi:[10.1021/jp910227x](https://doi.org/10.1021/jp910227x)
35. Wang CCD, Choy WCH, Duan C, Fung DDS, Sha WEI, Xie F-X, Huang F, Cao Y (2012) Optical and electrical effects of gold nanoparticles in the active layer of polymer solar cells. *J Mater Chem* 22(3):1206–1211
36. Duan CH, Wang CD, Liu SJ, Huang F, Choy CHW, Cao Y (2011) Two-dimensional like conjugated copolymers for high efficiency bulk-heterojunction solar cell application: band gap and energy level engineering. *Sci China Chem* 54(4):685–694
37. Mayer AC, Scully SR, Hardin BE, Rowell MW, McGehee MD (2007) Polymer-based solar cells. *Mater Today* 10:28–33
38. Mandoc MM (2007) Optimum charge carrier mobility in organic solar cells. *Appl Phys Lett* 90(13):133504
39. Mihailetchi VD, van Duren JKJ, Blom PWM, Hummelen JC, Janssen RAJ, Kroon JM, Rispens MT, Verhees WJH, Wienk MM (2003) Electron transport in a methanofullerene. *Adv Funct Mater* 13(1):43–46. doi:[10.1002/adfm.200390004](https://doi.org/10.1002/adfm.200390004)
40. Zhao DW (2009) An inverted organic solar cell with an ultrathin Ca electron-transporting layer and MoO₃ hole-transporting layer. *Appl Phys Lett* 95(15):153304
41. Jiang CY, Sun XW, Zhao DW, Kyaw AKK, Li YN (2010) Low work function metal modified ITO as cathode for inverted polymer solar cells. *Sol Energy Mater Sol Cells* 94(10):1618–1621. doi:[10.1016/j.solmat.2010.04.082](https://doi.org/10.1016/j.solmat.2010.04.082)
42. Koster LJA, Smits ECP, Mihailetchi VD, Blom PWM (2005) Device model for the operation of polymer/fullerene bulk heterojunction solar cells. *Phys Rev B* 72(8):085205
43. Zheng T, Choy WCH, Sun Y (2009) Hybrid nanoparticle/organic devices with strong resonant tunneling behaviors. *Adv Funct Mater* 19(16):2648–2653. doi:[10.1002/adfm.200900308](https://doi.org/10.1002/adfm.200900308)
44. Chen H-Y, Hou J, Zhang S, Liang Y, Yang G, Yang Y, Yu L, Wu Y, Li G (2009) Polymer solar cells with enhanced open-circuit voltage and efficiency. *Nat Photon* 3(11):649–653

45. Xu Z, Chen L-M, Yang G, Huang C-H, Hou J, Wu Y, Li G, Hsu C-S, Yang Y (2009) Vertical phase separation in poly(3-hexylthiophene): fullerene derivative blends and its advantage for inverted structure solar cells. *Adv Funct Mater* 19(8):1227–1234. doi:[10.1002/adfm.200801286](https://doi.org/10.1002/adfm.200801286)
46. Mihailtchi VD, Koster LJA, Hummelen JC, Blom PWM (2004) Photocurrent generation in polymer-fullerene bulk heterojunctions. *Phys Rev Lett* 93(21):216601
47. Chen F-C, Wu J-L, Lee C-L, Hong Y, Kuo C-H, Huang MH (2009) Plasmonic-enhanced polymer photovoltaic devices incorporating solution-processable metal nanoparticles. *Appl Phys Lett* 95(1):013305
48. Blom PWM, Mihailtchi VD, Koster LJA, Markov DE (2007) Device physics of polymer: fullerene bulk heterojunction solar cells. *Adv Mater* 19(12):1551–1566. doi:[10.1002/adma.200601093](https://doi.org/10.1002/adma.200601093)
49. Brabec CJ, Cravino A, Meissner D, Sariciftci NS, Fromherz T, Rispeins MT, Sanchez L, Hummelen JC (2001) Origin of the open circuit voltage of plastic solar cells. *Adv Funct Mater* 11(5):374–380. doi:[10.1002/1616-3028\(200110\)11:5<374:aid-adfm374>3.0.co;2-w](https://doi.org/10.1002/1616-3028(200110)11:5<374:aid-adfm374>3.0.co;2-w)
50. Vandewal K, Tvingstedt K, Gadisa A, Inganas O, Manca JV (2009) On the origin of the open-circuit voltage of polymer-fullerene solar cells. *Nat Mater* 8(11):904–909
51. Tress W, Leo K, Riede M (2011) Influence of hole-transport layers and donor materials on open-circuit voltage and shape of I-V curves of organic solar cells. *Adv Funct Mater* 21(11):2140–2149. doi:[10.1002/adfm.201002669](https://doi.org/10.1002/adfm.201002669)
52. Akaike K, Kanai K, Ouchi Y, Seki K (2010) Impact of ground-state charge transfer and polarization energy change on energy band offsets at donor/acceptor interface in organic photovoltaics. *Adv Funct Mater* 20(5):715–721. doi:[10.1002/adfm.200901585](https://doi.org/10.1002/adfm.200901585)
53. Sun B (2005) Vertically segregated hybrid blends for photovoltaic devices with improved efficiency. *J Appl Phys* 97(1):014914
54. Snaith HJ, Greenham NC, Friend RH (2004) The origin of collected charge and open-circuit voltage in blended polyfluorene photovoltaic devices. *Adv Mater* 16(18):1640–1645. doi:[10.1002/adma.200305766](https://doi.org/10.1002/adma.200305766)
55. Kim K, Carroll DL (2005) Roles of Au and Ag nanoparticles in efficiency enhancement of poly(3-octylthiophene)/C₆₀ bulk heterojunction photovoltaic devices. *Appl Phys Lett* 87(20):203113. doi:[10.1063/1.2128062](https://doi.org/10.1063/1.2128062)
56. Xie FX, Choy WCH, Wang CCD, Wei E, Fung DDS (2011) Improving the efficiency of polymer solar cells by incorporating gold nanoparticles into all polymer layers. *Appl Phys Lett* 99:153304
57. Peng B, Guo X, Cui C, Zou Y, Pan C, Li Y (2011) Performance improvement of polymer solar cells by using a solvent-treated poly(3,4-ethylenedioxythiophene): poly(styrenesulfonate) buffer layer. *Appl Phys Lett* 98(24):243308
58. Xie F, Choy WCH, Zhu X, Li X, Li Z, Liang C (2011) Improving polymer solar cell performances by manipulating the self-organization of polymer. *Appl Phys Lett* 98:243302
59. Sievers DW, Shrotriya V, Yang Y (2006) Modeling optical effects and thickness dependent current in polymer bulk-heterojunction solar cells. *J Appl Phys* 100:114509